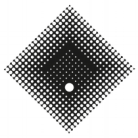
VICTORIA UNIVERSITY
MELBOURNE AUSTRALIA

Tests and finite element modeling of concrete beams reinforced with reused steel bars

This is the Published version of the following publication

Attia, Mohammed M, Abdelsalam, Bassam Abdelsalam, Eita, M. A, Ahmed, Mizan, Liang, Qing and Rageh, Basem O (2023) Tests and finite element modeling of concrete beams reinforced with reused steel bars. Structural Concrete. ISSN 1464-4177

The publisher's official version can be found at https://onlinelibrary.wiley.com/doi/10.1002/suco.202300316
Note that access to this version may require subscription.

Downloaded from VU Research Repository https://vuir.vu.edu.au/47416/

Check for updates

Received: 19 April 2023 | Revised: 10 August 2023 | Accepted: 28 September 2023

DOI: 10.1002/suco.202300316

ARTICLE

fib CEB-FIP WILEY

Tests and finite element modeling of concrete beams reinforced with reused steel bars

Mohammed M. Attia[1] | **Bassam Abdelsalam Abdelsalam**[1] | **M. A. Eita**[2] | **Mizan Ahmed**[3] | **Qing Quan Liang**[4] | **Basem O. Rageh**[5]

[1]Civil and Architecture Constructions Department, Faculty of Technology and Education, Suez University, Suez, Egypt

[2]The High Technological Institute, 10th of Ramadan City, Egypt

[3]Centre for Infrastructure Monitoing and Protection, School of Civil and Mechanical Engineering, Curtin University, Bentley, WA, Australia

[4]College of Sport, Health, and Engineering, Victoria University, Melbourne, Victoria, Australia

[5]Civil Engineering Department, Delta Higher Institute for Engineering and Technology, Mansoura, Egypt

Correspondence
Qing Quan Liang, College of Sport, Health, and Engineering, Victoria University, PO Box 14428, Melbourne VIC 8001, Australia.
Email: qing.liang@vu.edu.au

Abstract

This paper presents the experimental study and finite element modeling of the flexural behavior of concrete beams reinforced with reused steel bars as longitudinal reinforcements. The experimental program and results of eight reinforced concrete (RC) beams constructed with and without reused steel bars are described in detail. The replacement percentages of brand-new bars with reused steel bars in the tested beams were 50% and 100%. The reused steel bars were coated with and without epoxy. Steel fibers with fractions of 0.5% and 1.0% of the concrete volume were added to the concrete mixes. The load-deflection relationship, ductility index, toughness, and failure modes of the tested beams are presented and discussed. It is shown that utilizing reused steel bars decreases the ultimate load of RC beams but increases their deflection at the ultimate load compared with the control beam. Increasing the steel fiber ratio increases the ultimate load and the deflection at the ultimate load of RC beams incorporating reused steel bars. However, the zinc-rich epoxy used to coat the reused steel bars does not affect the behavior of the beams. Three-dimensional nonlinear finite element (FE) models of the tested beams were developed using ABAQUS and validated against the test results. The developed FE models are capable of accurately simulating the experimentally observed behavior of RC beams with reused steel bars.

KEYWORDS

finite element modeling, flexural behavior, reinforced concrete beams, reused steel bars, steel fibers

1 | INTRODUCTION

Because of its high mechanical and durability features, concrete is the most extensively used construction material in buildings, bridges, dams, and so forth.[1,2] Steel in different forms (bars, fibers, wires, meshes, etc.) has been used as reinforcement in reinforced concrete (RC) since its release in the mid-19th century. Steel rebars are the most effective kind of reinforcement for concrete; therefore, it has been extensively utilized in concrete structures. Rebar consumption is increasing due to the increase in the use of concrete. The construction sector

This is an open access article under the terms of the Creative Commons Attribution License, which permits use, distribution and reproduction in any medium, provided the original work is properly cited.
© 2023 The Authors. *Structural Concrete* published by John Wiley & Sons Ltd on behalf of International Federation for Structural Concrete.

consumes around 56% of world steel demand. It has been estimated that the steel industry produced about 25% of gas emissions, which are a major source of greenhouse gases. Reusing and recycling construction materials helps to decrease the waste, conserve natural resources, and reduce greenhouse gas emissions.[3,4] Several studies have revealed that towards the conclusion of a facility's life, 83% of steel is recycled, 14% is reused, and 3% is landfilled.[5] Incorporating reused reinforcing bars in new concrete structures can lead to a significant reduction in construction and material costs and environmental impacts associated with the production of new reinforcing bars. Tayeh et al.[5] studied the possibility of re-certification of reused steel bars collected from demolished construction sites to construct new houses in Gaza by performing tensile tests. It was found that the reused bars collected from ground beams passed all the tensile test requirements.

Steel fibers (SFs) are often used in concrete mixes to improve the mechanical performance of concrete, particularly its ductility. In the area where a fracture has formed, fibers serve as linkages that transfer stresses inside the concrete. SFs increase the energy absorption capacity of concrete and help to reduce the spread and expansion of the fractures in concrete. Ahmed et al.[6] presented a thorough review on the effects of recycled fibers on the mechanical properties and ductility of concrete. It was concluded that recycled fibers significantly improved the tensile and flexural strengths, the energy absorption, impact resistance, and ductility performance of recycled fiber concrete. Behbahani et al.[7] studied the effects of the addition of an optimum percentage of SFs on the flexural behavior of RC beams. The volume fractions of SFs used were 0%, 0.5%, 1%, 1.5%, and 2%. The experimental findings showed that the beams with SFs had higher cracking load, ultimate flexural strength, stiffness, and ductility than the ones without SFs. Prakash et al.[8] investigated the sensitivity of the flexural characteristics of coconut shell concrete partially blended with Fly Ash to SFs. The ultimate moment capacity of the RC beams was enhanced by 5%–14% by the inclusion of SFs. Mertol et al.[9] concluded that using fiber RC instead of conventional concrete improved the ultimate load and stiffness of the beams. Henager and Doherty[10] reported that the presence of SEs not only enhanced the ultimate load capacity and postcracking stiffness of the RC beam but also reduced the crack width.

Numerical models were also developed by researchers to study the behavior of RC members.[11–17] Hamoda et al.[14,15] developed finite element models (FEM) to study the flexural and shear behavior of RC beams strengthened with engineered cementitious composite and stainless-steel strips. Rageh et al.[12] developed FEM of RC beams strengthened with glass fiber reinforcement polymer subjected to flexural load. The FEM was found to accurately predict the experimentally observed performance of RC beams. Although extensive research studies have been performed to study the structural behavior of RC beams with SFs, no research has been undertaken to determine the behavior of RC beams utilizing reused steel bars as longitudinal reinforcements with or without SFs. This paper fills this research gap by performing tests on RC beams longitudinally reinforced with reused bars as well as developing FE models for simulating the behavior of such beams. The FE models are validated by experiments.

2 | RESEARCH SIGNIFICANCE

Egypt's steel production reached 5.80 million tons in 2022, which led to an increase in energy consumption and carbon emissions that affect climate change. The demolition of buildings due to violating building codes and defects in design and construction results in more waste. The environmental problems of production, the high cost of reinforcing steel bars, and the increase in demolition waste demand nontraditional and sustainable solutions. Possibility of incorporating reused reinforcing bars in new concrete structures such as in concrete beams can lead to a significant reduction in construction and material costs and environmental impacts associated with the production of new reinforcing bars. However, there has not been any research undertaken to study the behavior of concrete beams incorporating reused reinforcing bars. Therefore, this research focuses on studying the flexural behavior of RC beams containing reused steel bars obtained from building demolition as a replacement of brand-new bars. The influences of the percentage of reused bars in the section, the coating with an epoxy material, and the volume fractions of discrete SFs on the responses of RC beams are studied. The results obtained from this study will provide crucial information on the understanding of the effects of reused reinforcing bars on the performance of RC beams.

3 | EXPERIMENTAL PROGRAM

3.1 | Details of specimens

In the experimental program, eight simply supported rectangular RC beams were tested under flexural load up to failure using both reused and brand-new bars. All beams were 1500 mm long, had the same width-to-depth ratio (150/200 mm), and were reinforced with four longitudinal steel bars (SFs) with a diameter of 12 mm at the

17517648, 0, Downloaded from https://onlinelibrary.wiley.com/doi/10.1002/suco.202300316 by Victoria Universitaet, Wiley Online Library on [22/11/2023]. See the Terms and Conditions (https://onlinelibrary.wiley.com/terms-and-conditions) on Wiley Online Library for rules of use; OA articles are governed by the applicable Creative Commons License

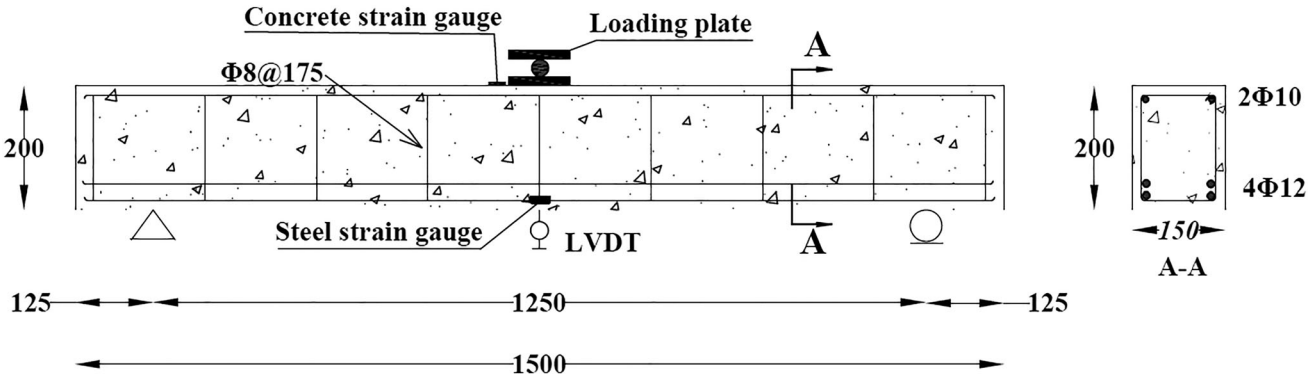

FIGURE 1 The geometrical and reinforcement details of beams.

TABLE 1 Details of the tested specimens.

No.	Beams	Reused steel (%)	Steel fiber	Epoxy	Rebars	Stirrups
1	B0-0RS	0	—	—	12 Ø4	Ø8 @175 mm
2	B1-50RS	50	—	—		
3	B2-100RS	100	—	—		
4	B3-100RS-Ep	100	—	Ep		
5	B4-100RS-0.5SF	100	0.5	—		
6	B5-100RS- 1SF	100	1	—		
7	B6-100RS-0.5SF-Ep	100	0.5	Ep		
8	B7-100RS-1SF-Ep	100	1	Ep		

bottom and two of 10 mm at the top. The stirrups in all beams were rectangular shape of 8 mm steel bars separated at 175 mm to prevent shear failure. Figure 1 illustrates the geometry and reinforcing details of the tested beams. In the naming of the beams, the letter "B" followed by the number refers to the number of the specimen, the number (0–100) next to the letter "RS" refers to the ratio of reused steel rebars used in the specimen, the number (0.5–1.0) next to letter "SF" refers to the ratio of SFs used in the specimen and the letter "Ep" refers to the reused steel rebars coated with zinc-rich epoxy from Sika Egypt. As illustrated in Table 1, the beam B0-0RS served as the reference control beam. The beams B0-0RS, B1-50RS, and B2-100RS contained 0%, 50%, and 100% reused steel rebars, respectively. The beams B4-100RS-0.5SF, and B5-100RS-1SF, contained 0.5%, and 1% SFs, respectively. The beams B3-100RS-Ep, B6-100RS-0.5SF-Ep, and B7-100RS-1SF-Ep contained 0%, 0.5%, and 1% SFs, respectively, and were made of reused steel rebar coated with zinc-rich epoxy. It should be noted that Zinc-rich coatings require surface preparation, which involves abrasive blasting or other methods to clean and roughen the surface of the steel bars. This roughened surface provides a better mechanical bond with the surrounding concrete, improving the adhesion between the two materials. When zinc-rich coatings are used along with steel bars, they create a galvanic effect. In the presence of moisture or when the concrete is exposed to chloride ions, the zinc coating corrodes preferentially over the steel. This cathodic protection of the steel bars further reduces the risk of corrosion, which can weaken the bond between the steel and the concrete.

3.2 | Material properties of SFRC

The traditional hydraulic cement, fine and coarse aggregates, water, super-plasticizers (SP), chemical admixtures, and discrete discontinuous SFs were all used to make SFRC. Locally available ordinary Portland cement of grade 42.5 N was used. The Blaine fineness of this cement was 3255 cm^2/g, and the specific gravity was 3.15. Table 2 presents the physical characteristics, phase composition, and chemical properties of the cement. The SFRC mixes used aggregates that were available locally. The river sand's specific gravity, water absorption, and fineness modulus were all 2.57 g/cm^3, 1.90%, and 2.89, respectively. A stone that had been naturally crushed and had a nominal maximum size of 20 mm was utilized as the

17517648, 0, Downloaded from https://onlinelibrary.wiley.com/doi/10.1002/suco.202300316 by Victoria Universitaet, Wiley Online Library on [22/11/2023]. See the Terms and Conditions (https://onlinelibrary.wiley.com/terms-and-conditions) on Wiley Online Library for rules of use; OA articles are governed by the applicable Creative Commons License

Physical properties		Chemical properties (%)	
Water for standard consistency (%)	27.2	CaO	63.64
Specific surface area-Blain (cm^2/g)	3255	SiO_2	19.58
Specific weight	3.15	Al_2O_3	5.41
Soundness—Le-Chatelier (mm)	1.5	Fe_2O_3	3.41
Initial setting time (min.)	150	SO_3	2.29
Final setting time (min.)	189	MgO	0.91
Phase composition (%)		K_2O	—
C_3S	68.11	Na_2O	0.83
C_2S	4.64	Cl	0.048
C_3A	6.56	F-CaO	1.1
C_4AF	10.22	LOI	4.65

TABLE 2 Physical properties and chemical composition of cement.

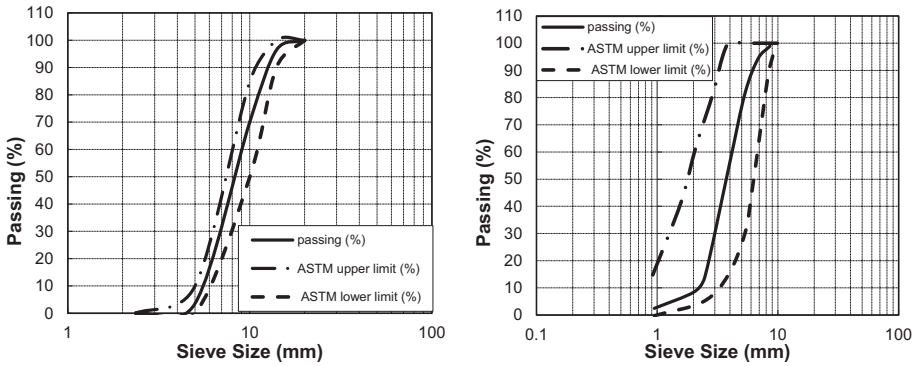

(a) Coarse aggregate (b) Fine aggregate

FIGURE 2 Sieve analysis of fine and coarse aggregates. (a) Coarse aggregate. (b) Fine aggregate.

coarse aggregate. The specific gravity and water absorption of the coarse aggregate were 2.75 g/cm^3 and 1.43%, respectively. The aggregate grading curves are depicted in Figure 2. Sikament®−NN from sika Egypt was used, which was a sulfonated naphthalene formaldehyde-type SP with a specific gravity of 1.2 and a pH of more than 6 to assure the workability and prevent the balling impact of fibers. As shown in Figure 3, Hooked-end SFs from Nassar Group Company in Egypt with a 50-aspect ratio, a length of 50 mm, and a diameter comparable to 1 mm were employed. The fiber had a density of 7850 kg/m^3, with volume fractions of 0%, 0.5%, and 1%. It should be noted that according to ACI 544,[20] the typical volume fractions used for casting SFRC range from 0.25% to 1.5% of the total volume. The addition of SFs may reduce the slump of the composite as compared with a non-fibrous mixture in the range. The tensile strength and elastic modulus of fiber were 1100 MPa and 210 GPa, respectively. M0, M0.5, and M1 were three mixes used that comprise 0%, 0.5%, and 1% SFs by volume of concrete, respectively. The proportions of the concrete mixes are given in Table 3.

3.3 | Material properties of reinforcing steel

Brand-new and reused steel bars were used as reinforcing steel in the tested beams. The reused bars were obtained from collapsed constructions with no corrosion or damage to the bar ribs as illustrated in Figure 4. Reused bars were prepared by following the steps: straightening the rebars, eliminating concrete residues, and coating it with Sika Zinc Rich®−2 epoxy from Sika Egypt. This preparation provided excellent protection against corrosion for rebars and excellent adhesion between reinforcement bars and concrete. The properties of Sika Zinc Rich®−2 are given in Table 4. The tensile test was performed on each steel bar to determine the steel grade in accordance with ASTM A370 standards,[18] as shown in Figure 5. The material properties of the reused and brand-new bars are given in Table 5.

Pull-out tests on both brand-new and reused steel bars were performed to investigate their bond strengths. The pullout test was performed in accordance with British Standard 5080: Part 1: 1993.[19] Brand-new and

17517648, 0, Downloaded from https://onlinelibrary.wiley.com/doi/10.1002/suco.202300316 by Victoria Universitaet, Wiley Online Library on [22/11/2023]. See the Terms and Conditions (https://onlinelibrary.wiley.com/terms-and-conditions) on Wiley Online Library for rules of use; OA articles are governed by the applicable Creative Commons License

reused bars were placed in the center of freshly cast 300-mm concrete cylinders, cured until the concrete reached its full strength, and then tested. Figure 6 illustrates the test setup of the pullout test and its results, respectively.

3.4 | Specimen preparation

The beam specimens were cast in wooden molds, and reinforcing cages were manufactured and installed in the molds, as illustrated in Figure 7. For the beams which contained reused steel, the reused steel was placed in the second layer. The concrete mix design was performed based on ACI 544.[20] Specimens were demolded after 24 h and cured for 28 days in damp gunny bags to avoid moisture loss. Nine cylinders of 150 × 300 mm size were cast alongside the beams to determine their compressive strength, tensile strength, and modulus of elasticity of concrete as shown in Figure 8. The measured compressive and tensile strengths of the concrete are given in Table 3. The typical compressive stress–strain relationships obtained experimentally for the three considered concrete mixtures are illustrated in Figure 8c.

3.5 | Test setup and instrumentation

All the beams were tested utilizing a universal testing machine (UTM) with a hinge at 125 mm from the end support and a roller at 125 mm from the opposite side support under one-point loading, as shown in Figure 9. A uniaxial compressive load of 3000 kN was applied in a monotonic manner using a UTM. To measure the deflection, linear variable differential transducers with a precision of 0.01 mm were placed in the center of the beam. As shown in Figure 9, electronic strain gauges were installed on the internal longitudinal steel bars and the concrete surface of each beam to detect stresses in the tension and compression zones. The load was applied at 0.50 mm/min continuously until the ultimate load was reached. During the test, the cracks that formed on the beam's surface were marked and both deformation and strains were monitored until the beam failed.

4 | RESULTS AND DISCUSSIONS

4.1 | Load-deflection behavior

Table 6 and Figure 10a show a comparison of the ultimate loads and corresponding deflections values for all

FIGURE 3 Hoked-Steel Fiber.

FIGURE 4 Samples of the reused bars.

TABLE 3 Proportions and properties of concrete.

	Ingredient of mixtures (kg)					Properties of mixtures (MPa)	
Mix ID	Cement	Fine aggregates	Coarse aggregates	Water	SP	Compressive strength (F_c)	Tensile strength (F_{ct})
Mo	520	857.83	1286.74	180	8	48.15	3.20
M0.5	520	851.21	1276.81	180	8	49.20	3.82
M1.0	520	844.58	1266.87	180	8	50.43	4.16

Abbreviation: SP, super-plasticizers.

17517648, 0, Downloaded from https://onlinelibrary.wiley.com/doi/10.1002/suco.202300316 by Victoria Universitaet, Wiley Online Library on [22/11/2023]. See the Terms and Conditions (https://onlinelibrary.wiley.com/terms-and-conditions) on Wiley Online Library for rules of use; OA articles are governed by the applicable Creative Commons License

beams. The structural behavior of RC beams is affected by the amount of reused steel rebars, as presented in Figure 10a. The behavior of the tested beams is analyzed by comparison with the control beam B0-0RS, which contained 100% new-brand steel bars and had the ultimate load of 104.60 kN and the deflection of 7.70 mm. All the beams demonstrated a steep linear elastic behavior prior to the onset of the first flexural cracks as shown in Figure 9. The longitudinal steel bars yielded when the load was increased. When the applied load was increased further, the beam finally collapsed, and the concrete crushed in the compression zone. In the first group, the deflection of specimens B1-50RS and B2-100RS increases by 19% and 24%, respectively when compared with the control beam B0-0RS. On the other hand, the ultimate loads of B1-50RS and B2-100RS are 91.90 and 84.90 kN, which decrease by 12% and 19%, respectively, compared with the control beam, as shown in Figure 10b. Although the reused steel bars had higher tensile strength than the brand-new steel bars, they had lower yield stress and stiffness than the brand-new steel bars. The yield and ultimate loads and ductility of RC beams with reused steel bars under bending were lower than those of the control beam. This means that the higher tensile strength of reused steel bars was not fully utilized in the RC beams.

In the second group, the beams B4-100RS-0.5SF and B5-100RS-1SF, which were reinforced with 100% reused steel bars and included 0.5% and 1% SFs, have higher ultimate loads and larger deformations than B2-100RS as depicted in Figure 10c. The use of 100% reused bars with 1% SFs enhances the ultimate load by 6.3% in comparison with the control beam B0-0RS. In addition, the deformations of beams B4 with 0.5% SFs and B5 having 1% SFs are 30.4% and 48.5% larger than that of the control beam, respectively. Although adding SFs to beams B4 and B5 improves their performance, their strength and stiffness are still lower than those of control beam.

The load-deflection responses of beams B3-100RS-Ep, B6-100RS-0.5%SF-Ep, and B7-100RS-1%SF-Ep in which the reused bars were coated with epoxy are presented in Figure 9d. It can be seen from Figure 9a,c,d that the zinc-rich epoxy does not have a noticeable effect on the behavior of RC beams. The ultimate load of B7-100RS-1%SF-Ep is 8.1% and 33.2% higher than that of B0-0RS and B2-100RS, respectively due to the addition of more SFs. The deformations at the ultimate load of beams B3, B6, and B7 are shown to increase by 19.5%, 27.6%, and 42.3%, respectively compared with the beam B0-0RS. This is attributed to the fact that the addition of SFs markedly reduces the concrete cracks, thereby increasing the flexural strength and displacement ductility of RC beams.

TABLE 4 Proportions of concrete Sika Zinc Rich®−2.

Composition	Epoxy modified zinc
Mixing Ratio	Comp. (A: B) by wt. = 5: 1
Color	Metal Gray
Density	1.78 Kg/L
Drying Stage	40 min

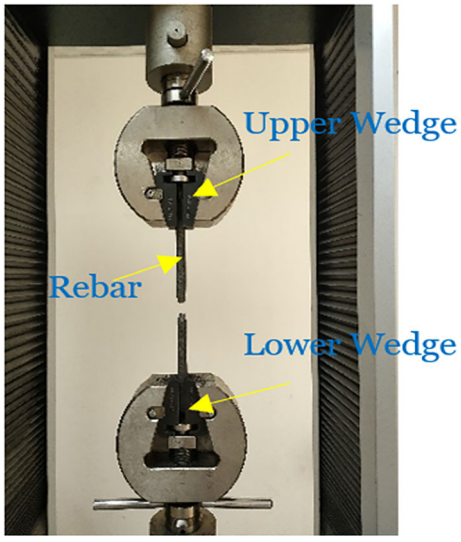

FIGURE 5 Tensile test of steel bars.

4.2 | Ductility index and toughness

The ductility index (μ) can be expressed as the ratio of the displacement (Δ_u) at the load that falls to 85% of the

TABLE 5 Mechanical characteristics of brand-new and reused bars.

Steel type	Diameter (mm)	Elastic modulus (GPA)	Yield stress (MPa)	Ultimate stress MPa	Ultimate strain
Brand-new	10	208	420	520	0.13
Brand-new	12	210	425	555	0.14
Reused	12	106	380	580	0.12

17517648, 0, Downloaded from https://onlinelibrary.wiley.com/doi/10.1002/suco.202300316 by Victoria Universitaet, Wiley Online Library on [22/11/2023]. See the Terms and Conditions (https://onlinelibrary.wiley.com/terms-and-conditions) on Wiley Online Library for rules of use; OA articles are governed by the applicable Creative Commons License

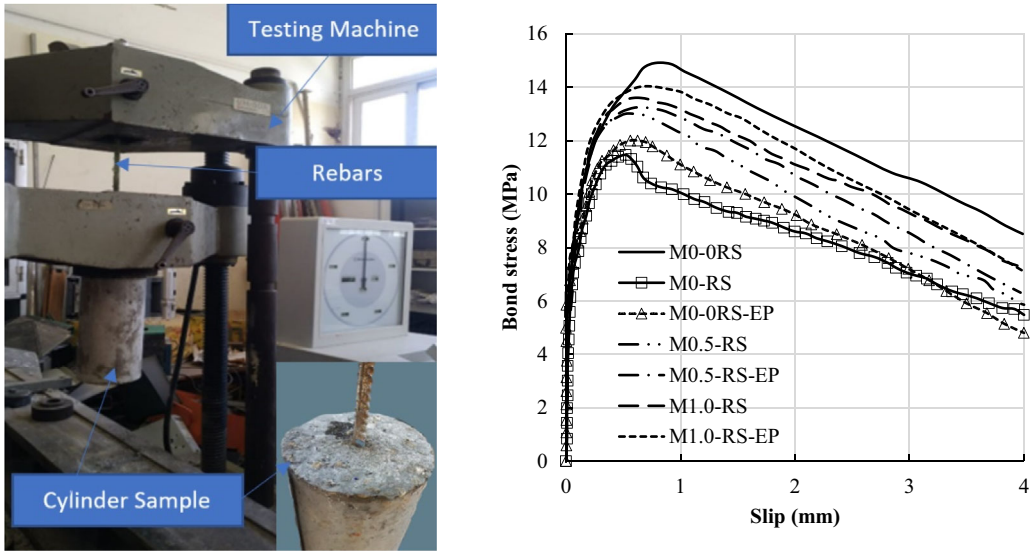

FIGURE 6 Pull-out tests on both reinforcement bars. (a) Test setup. (b) Bond-slip curves.

FIGURE 7 Fabricated beams samples. (a) Wooden molds. (b) Reinforcement cages.

(a) Wooden molds (b) Reinforcement cages

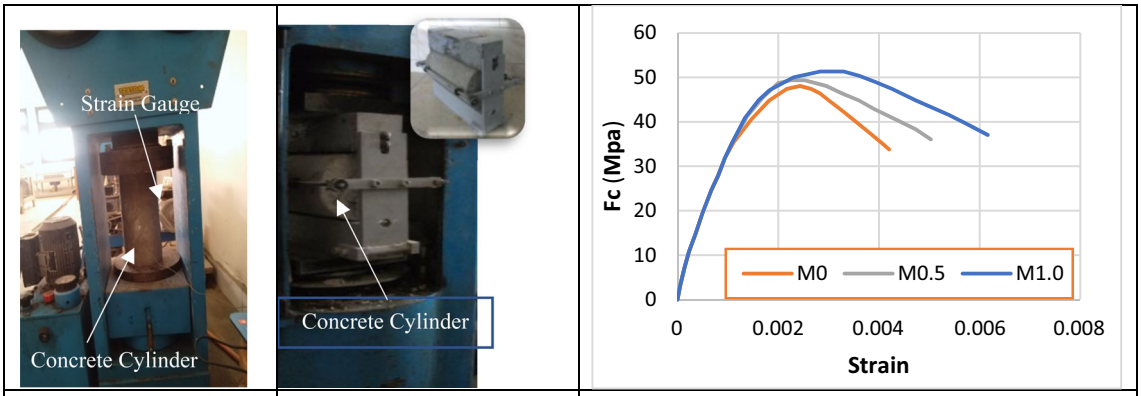

FIGURE 8 Concrete tests: (a) compressive test, (b) splitting test, and (c) compressive stress–strain of the concrete.

ultimate load (P_u) to the displacement at yield load (Δ_y).[21] The ultimate state is defined as the point at which the beam cannot sustain additional deformation at the same load intensity.[22] As a rule of thumb, a ductility index of <35% represents brittle failure. Table 6 and Figure 11a show the ductility index results of all tested beams. It is shown that the ductility indices of all beams, except B5-100RS-1SF and B7-100RS-1SF-Ep, are between 1.91 and 2.18, which are slightly less than that of the control beam B0-0RS (2.27). The addition of 1% SFs to beams B5 and B7 improves their ductility index by 26.9% and 25.1%, respectively, compared with the control beam. Both the reused steel bars and zinc-rich epoxy do not decrease the ductility index.

The area under the load-deflection graph for a beam is the flexural toughness. Table 6 and Figure 11b show the flexural toughness values calculated for each beam. The calculated toughness values of beams B0-0RS, B1-50RS, and B2-100RS are 586, 618, and 579 kN mm, respectively. When 50% of the steel bars are reused bars, the toughness

17517648, 0, Downloaded from https://onlinelibrary.wiley.com/doi/10.1002/suco.202300316 by Victoria Universitaet, Wiley Online Library on [22/11/2023]. See the Terms and Conditions (https://onlinelibrary.wiley.com/terms-and-conditions) on Wiley Online Library for rules of use; OA articles are governed by the applicable Creative Commons License

increases by about 5.5% compared with the control beam B0-0RS. SFs contribute to the improvement in the toughness of RC beams. Mertol et al.[9] concluded that for over-reinforced sections, the difference between the flexural toughness of FRC specimens and traditional concrete specimens is significantly greater. The beams B4-100RS-0.5SF and B6-100RS-0.5SF-Ep, which incorporated 0.5% of SFs, have a higher toughness of 9.1% and 13.6% than the control beam. The toughness values of beams B5-100RS-1SF and B7-100RS-1SF-Ep, which contained 1% SFs, are 907 and 847 kN mm, respectively, indicating 54.7% and 44.6% increases compared with the control beam.

4.3 | Cracking and failure modes

The cracking patterns of the tested beams are shown in Figure 12. It can be observed that all beams behaved similarly in terms of crack progression, except cracking space. The cracks of beams that contained SFs were closer to each other than those of other beams. The first flexural crack appeared in the region of the maximum moment in the testing beam. As the load continued to increase, more flexural cracks developed in the regions between the loading point and supports. Most of the flexural cracks developed vertically as the applied load was increased further, and then inclined flexure-shear cracks started to appear. The crack distribution and shape at failure for all beams are visually compared in Figure 12. In contrast to the gradual crushing of concrete observed in the fiber-RC beams, a sudden crushing of concrete was observed in the conventional concrete beams. The use of reused steel bars decreases the number of cracks and crack distances in beams B1-50RS and B2-100RS.

The beam B3-100RS-Ep exhibits a good distribution of cracks along the length of the beam with more cracks than beams B1 and B2. The zinc-rich epoxy coating has improved the bonding performance in the interfacial zone between the reused steel bars and concrete. It is found that adding SFs to the concrete mix increases the deformations at the ultimate loads of the beams B4-100RS-0.5SF and B5-100RS-1SF. The tensile strength of the concrete mixture was increased by increasing the amount of SFs, as revealed in Table 3, consequently reducing the cracks in the RC beams. According to ACI Committee 544,[20] the addition of SFs reduces both micro- and macrocracking in the concrete matrix, which enhances the mechanical properties. However, the ductility and flexural toughness properties of concrete depend on the volume fraction, aspect ratio, and type of fiber used. SFs typically make concrete matrix less brittle, but they have little or no impact on the capacity of the members.[23] According to Altun et al.,[24] RC beams with SFs have better behavior than beams made of conventional concrete in terms of the initiation, size, and propagation of flexural cracks. Furthermore, the epoxy coating in the reused steel bars (B6-100RS-0.5SF-Ep and B7-100RS-1SF-Ep) has no effects on crack development compared with

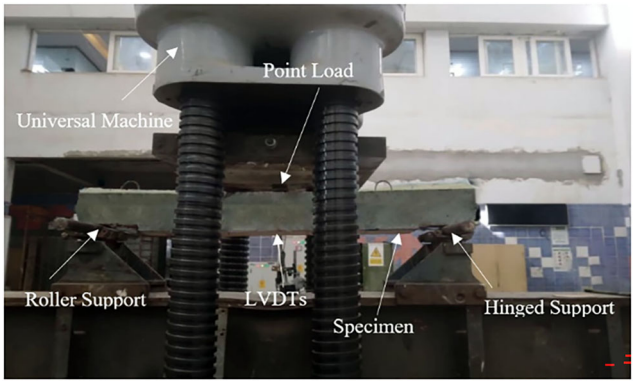

FIGURE 9 Test setup of reinforced concrete beam. LVDT, linear variable differential transducer.

TABLE 6 Experimental results of RC beams.

Beams ID	Loads (kN)		(Δy) mm	(Δu) mm	Toughness (kN.mm)	Ductility index (μ)
	Yield (Py)	Ultimate (Pu)				
B0-0RS	79.9	104.6	3.39	7.7	586	2.27
B1-50RS	74.5	91.9	4.33	9.2	618	2.12
B2-100RS	68.9	84.9	5.02	9.6	579	1.91
B3-100RS-Ep	67.4	85.9	4.53	9.2	567	2.03
B4-100RS-0.5SF	71.0	95.3	4.72	10.1	639	2.14
B5-100RS-1SF	72.8	111.2	3.99	11.5	907	2.88
B6-100RS-0.5SF-Ep	70.9	96.6	4.54	9.9	666	2.18
B7-100RS-1SF-Ep	72.2	113.1	3.87	11.0	847	2.84

17517648, 0, Downloaded from https://onlinelibrary.wiley.com/doi/10.1002/suco.202300316 by Victoria Universitaet, Wiley Online Library on [22/11/2023]. See the Terms and Conditions (https://onlinelibrary.wiley.com/terms-and-conditions) on Wiley Online Library for rules of use; OA articles are governed by the applicable Creative Commons License

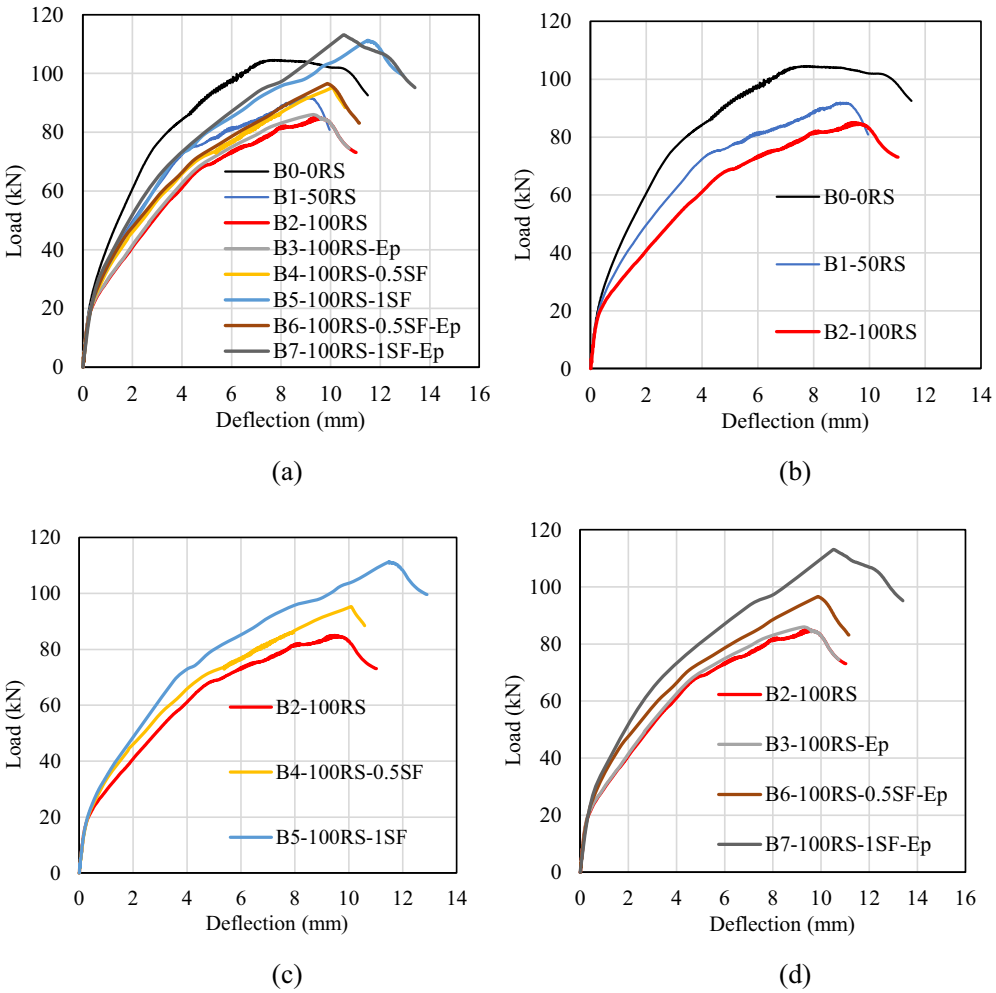

FIGURE 10 Load–deflection behavior of tested beams: (a) all tested reinforced concrete beams; (b) 50% and 100% reused steel (RS), (c) 100% RS with 0.5% and 1% Steel fibers (SFs), and (d) 100% RS coated by Ep with 0.5%, 1% SFs.

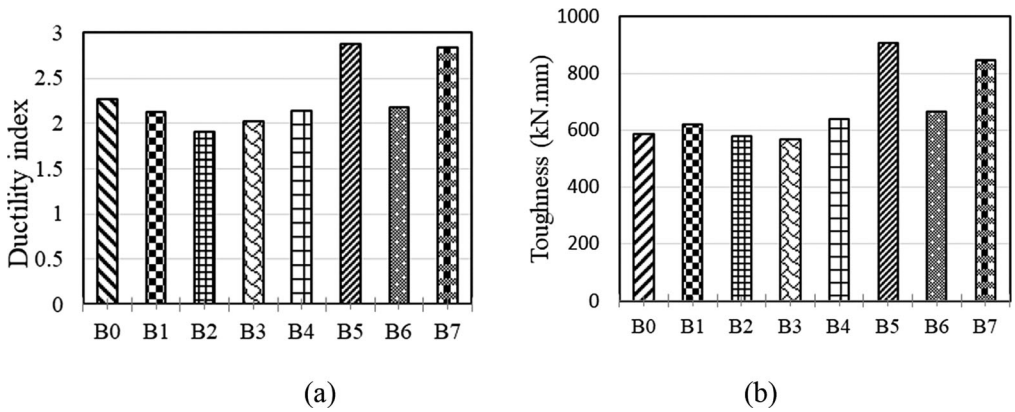

FIGURE 11 Ductility index and toughness results of all tested specimens.

B4 and B5 without epoxy, which have the same ratio of SFs.

5 | NUMERICAL MODELING

In this section, the FE analysis is performed to demonstrate the modeling of reused steel bars in RC concrete beam using FE software ABAQUS. The model assembly of concrete and reinforcement is shown in Figure 12.

5.1 | Modeling of materials

The concrete damage-plasticity model (CDP) was used to model the nonlinear behavior of concrete. The uniaxial

17517648, 0, Downloaded from https://onlinelibrary.wiley.com/doi/10.1002/suco.202300316 by Victoria Universitaet, Wiley Online Library on [22/11/2023]. See the Terms and Conditions (https://onlinelibrary.wiley.com/terms-and-conditions) on Wiley Online Library for rules of use; OA articles are governed by the applicable Creative Commons License

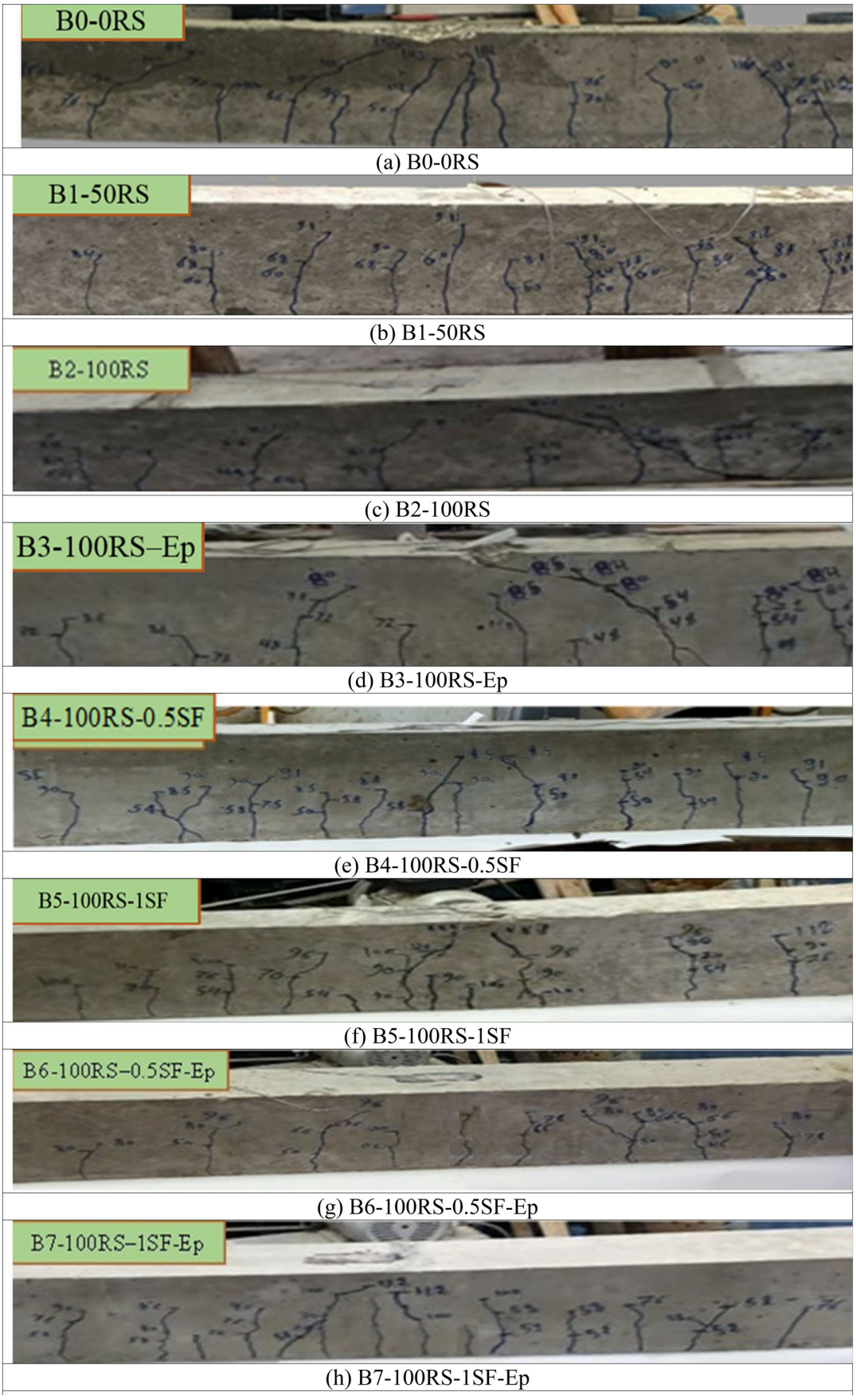

FIGURE 12 Failure modes of tested beams.

17517648, 0, Downloaded from https://onlinelibrary.wiley.com/doi/10.1002/suco.202300316 by Victoria Universitaet, Wiley Online Library on [22/11/2023]. See the Terms and Conditions (https://onlinelibrary.wiley.com/terms-and-conditions) on Wiley Online Library for rules of use; OA articles are governed by the applicable Creative Commons License

compression test results were used in the CDP model to simulate the compressive behavior of each concrete mix based on the experimental results (see Figure 8c and Table 3). Stress-fracture energy was employed to define tensile behavior of concrete. To avoid unreasonable mesh-sensitive outputs, the tensile postfailure behavior was specified in terms of a fracture energy-cracking criterion instead of a stress–strain curve. The postcracking stress-displacement curve for all tested beams is illustrated in Figure 14, where f_{ct} is the tensile stress of concrete and the fracture energy G_f is the area under the softening curve. This technique has been adopted widely in other studies.[25,26] The fracture energy G_f is calculated using CEB-FIP,[27] dependent on the concrete quality and the aggregate size. The tensile stress values f_{ct} of concrete for each mix used for constructing the postpeak stress deformation relationship were based on the splitting test results (see Table 3). In the CDP model, the Poisson's ratio (ν) of concrete was taken as 0.2, Dilation Angle (ψ) as 35°, $K = 0.667$, and eccentricity $\epsilon = 1$.

Typical bilinear (BL) elastic–plastic stress–strain curve depicted in Figure 15 was used to simulate the behavior of steel. The Poisson's ratio (ν) of steel was taken as 0.3 in the numerical modeling.

5.2 | Mesh and boundary conditions

The loads were applied on the elements that modeled the steel rigid plate with dimensions 150 mm × 75 mm × 25 mm as shown in Figure 13. Furthermore, the same dimensions were used for the steel supporting plates where the right support was modeled as hinged support and the left was a roller, as shown in Figure 13. As seen in Figure 16, the brick element C3D8R (cube 3D eight node-reduced integration) was used to model each concrete specimen. Three models with different mesh sizes, such as fine, medium, and coarse of 15, 25, and 35 mm, respectively, were studied to select a suitable mesh for accurately predicting the ultimate load and maximum deflection. The concrete medium volume meshes were ultilized in the finite element analysis (FEA) as shown in Figure 16. A two-noded linear 3D truss element (T3D2) was selected to model the brand-new bars and stirrups. To account for the bond between the tension steel bars and the surrounding concrete, the 3D eight-node brick element (C3D8R) was used to simulate the tensile bars (reused bars and reused bars with epoxy).

5.3 | Modeling of interaction between steel bars and concrete

To accurately simulate the behavior of tested RC beams, it is important to incorporate the mechanical interactions between the concrete and the embedded steel reinforcement. The embedded region approach has commonly been used. However, this method does not allow for the modeling of debonding between the steel and concrete. Therefore, to overcome this problem, the cohesive surface as shown in Figure 17 was considered in the FE model to

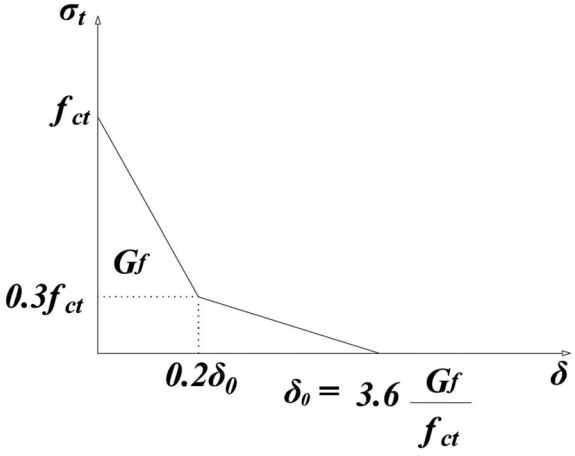

FIGURE 14 Postpeak stress deformation relationship of concrete under uniaxial tension.

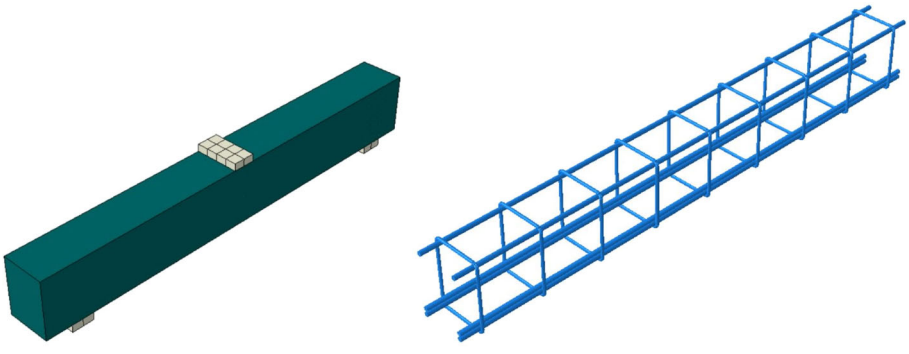

(a) 3D-Modeling of specimen (b) Steel bars and stirrups

FIGURE 13 Model assembly for studied specimen. (a) 3D-Modeling of specimen (b) Steel bars and stirrups.

17517648, 0, Downloaded from https://onlinelibrary.wiley.com/doi/10.1002/suco.202300316 by Victoria Universitaet, Wiley Online Library on [22/11/2023]. See the Terms and Conditions (https://onlinelibrary.wiley.com/terms-and-conditions) on Wiley Online Library for rules of use; OA articles are governed by the applicable Creative Commons License

simulate the bond-slip as a real contact between the reused steel bars and surrounding concrete.

In this modeling technique, the surface-based cohesive behavior requires a linear elastic traction separation as well as damage initiation and evolution laws. For the initiation of cohesive damage, quadratic traction function constraints with nominal stresses, as described in Equation (1), are as follows[28]:

$$\left\{\frac{\sigma_n}{\sigma_n^0}\right\}^2+\left\{\frac{\tau_n}{\tau_s^0}\right\}^2+\left\{\frac{\tau_t}{\tau_t^0}\right\}^2=1 \quad (1)$$

where σ_n is the cohesive tensile and τ_s and τ_t are shear stresses of the interface, and n, s, and t denote the direction of the stress component. Damage was considered to initiate when the traction function reached one. The values of shear stresses and the corresponding slip values were extracted from the pullout-test and used as input in the quadratic traction function. A BL constitutive model as shown in Figure 18 was used in this investigation to calculate the interface damage evolution and expressed in terms of energy release (Gf). Table 7 presents the input values used to simulate the interaction between the longitudinal bars in the flexural zone, based on the experimental results of pullout test (see Figure 5b). The equations of the BL bond-slip model are expressed as follows[29]:

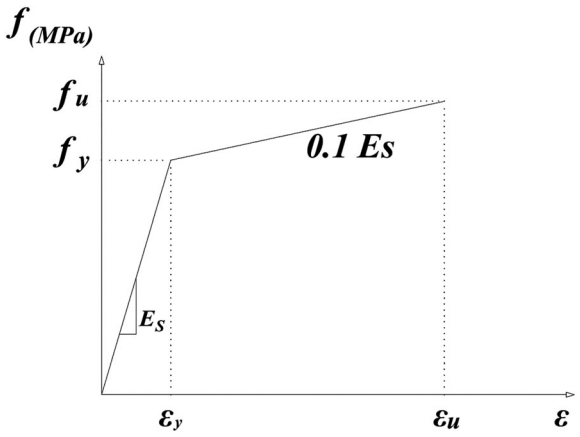

FIGURE 15 Stress–strain curve for brand new and reused steel bars in finite element analysis.

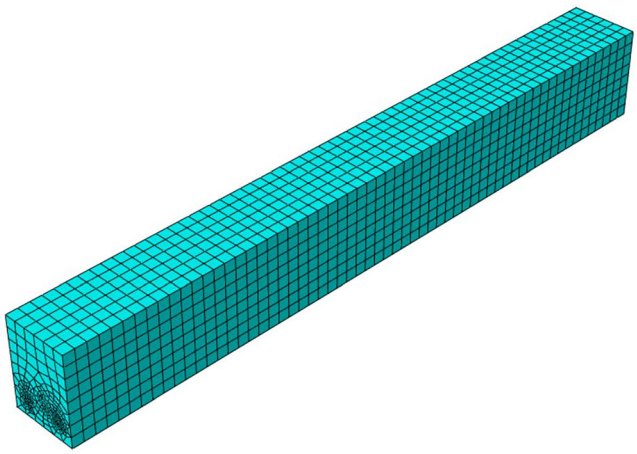

FIGURE 16 Meshing of the tested specimen in finite element analysis: mesh 25 × 25 mm.

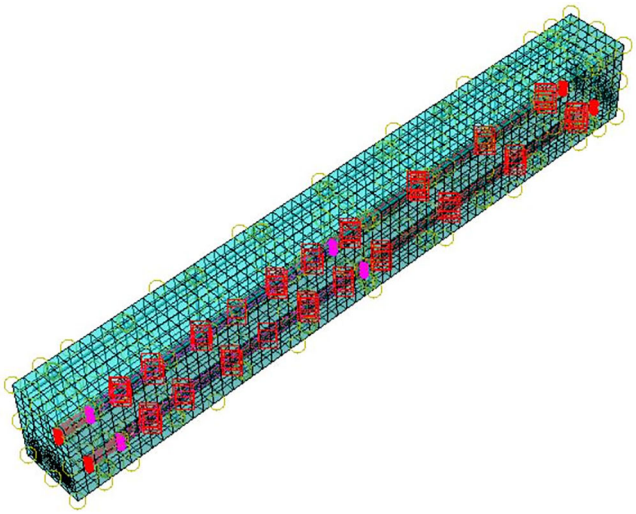

FIGURE 17 The interaction between the tension steel bars and the surrounding concrete (Cohesive contact).

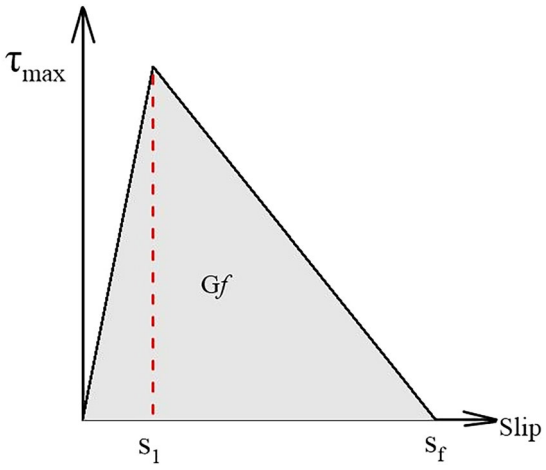

FIGURE 18 Bilinear bond-slip constitutive model. Note that τ, bond–shear stress; S, slip; τmax, maximum bond–shear stress; S1, slip at the achieved bond–shear stress; Sf, maximum slip of the bonded joint.

17517648, 0, Downloaded from https://onlinelibrary.wiley.com/doi/10.1002/suco.202300316 by Victoria Universitaet, Wiley Online Library on [22/11/2023]. See the Terms and Conditions (https://onlinelibrary.wiley.com/terms-and-conditions) on Wiley Online Library for rules of use; OA articles are governed by the applicable Creative Commons License

TABLE 7 Numerical input parameters for simulating the interaction between steel bars and surrounding concrete in all tested beams.

	Experimental values			Numerical input values				
				Quadratic traction function parameters		Bilinear bond-slip model parameters		
Beams ID	Concrete tensile strength (F_{ct}) (MPa)	Bond stress (τ_{max}) (MPa)	Slip (mm)	The cohesive tensile (σn^0) (MPa)	The shear stresses of the interface $\tau_s{}^0 = \tau_t{}^0$ (MPa)	(S_1) (mm)	(S_f) (mm)	Interfacial fracture energy (G_f) (N/mm)
B0-0RS	3.20	14.86	0.90	3.20	14.86	0.90	3.98	33.396
B1-50RS	3.20	11.46	0.53	3.20	11.46	0.53		25.51
B2-100RS	3.20	11.46	0.53	3.20	11.46	0.53		25.51
B3-100RS-Ep	3.20	12.0	0.61	3.20	12.0	0.61		26.82
B4-100RS-0.5SF	3.82	12.98	0.74	3.82	12.98	0.74		28.06
B5-100RS-1SF	4.16	13.59	0.81	4.16	13.59	0.81		32.13
B6-100RS-0.5SF-Ep	3.82	13.12	0.79	3.82	13.12	0.79		30.52
B7-100RS-1SF-Ep	4.16	14.10	0.84	4.16	14.10	0.84		32.56

TABLE 8 Comparison between the experimental and FE results.

	Ultimate load (kN)			Max. deflection (Δ_u) mm		
Beams	Test	FEM	Test/FEM	Test	FEM	Test/FEM
B0-0RS	104.6	105.51	0.99	7.7	9.8	0.79
B1-50RS	91.9	93.27	0.98	9.2	8.32	1.11
B2-100RS	84.9	87.8	0.96	9.6	9.04	1.06
B3-100RS-Ep	85.9	87.7	0.97	9.2	9.6	0.95
B4-100RS-0.5SF	95.3	97.1	0.98	10.1	9.7	1.04
B5-100RS-1SF	111.2	100.78	0.96	11.5	9.8	1.01
B6-100RS-0.5SF-Ep	96.6	112.59	0.98	9.9	11.7	0.98
B7-100RS-1SF-Ep	113.1	111.96	1.01	11.0	12.1	0.90
Mean			0.98			0.98
Standard deviation			0.02			0.10

Abbreviations: FE, finite element; FEM, finite element models.

$$\tau(s) = \begin{cases} \tau_{max} * \dfrac{s}{s_1}, & s < s_1 \\ \tau_{max} * \dfrac{(s_f - s)}{(s_f - s_1)}, & s > s_1 \text{ and } s \le s_f \\ 0, & s \ge s_f \end{cases} \quad (2)$$

5.4 | Convergence

Using the cohesive contact in FEA may cause convergence problems in the static nonlinear analysis. Therefore, the explicit dynamic solver was adopted in this study. This solver is successful due to the fewer convergence problems; furthermore, it is suitable for materials like concrete in terms of capturing concrete cracks and overall failure behavior.[30] The overall deflection was divided into a series of deflection increments in this investigation. At the end of each deflection increment, the adopted Newton–Raphson method enabled convergence within tolerance limits. The deflections were gradually increased in smaller increments during concrete cracking, steel yielding, and the last stage where cracks appear.

5.5 | Validation of the numerical modeling

The accuracy of the FE model is validated by comparing FE results with the ultimate load and maximum deflection of the tested beams obtained from the tests in Table 8. It can be seen that the FEM can accurately predict the ultimate loads and corresponding deflections of

17517648, 0, Downloaded from https://onlinelibrary.wiley.com/doi/10.1002/suco.202300316 by Victoria Universitaet, Wiley Online Library on [22/11/2023]. See the Terms and Conditions (https://onlinelibrary.wiley.com/terms-and-conditions) on Wiley Online Library for rules of use; OA articles are governed by the applicable Creative Commons License

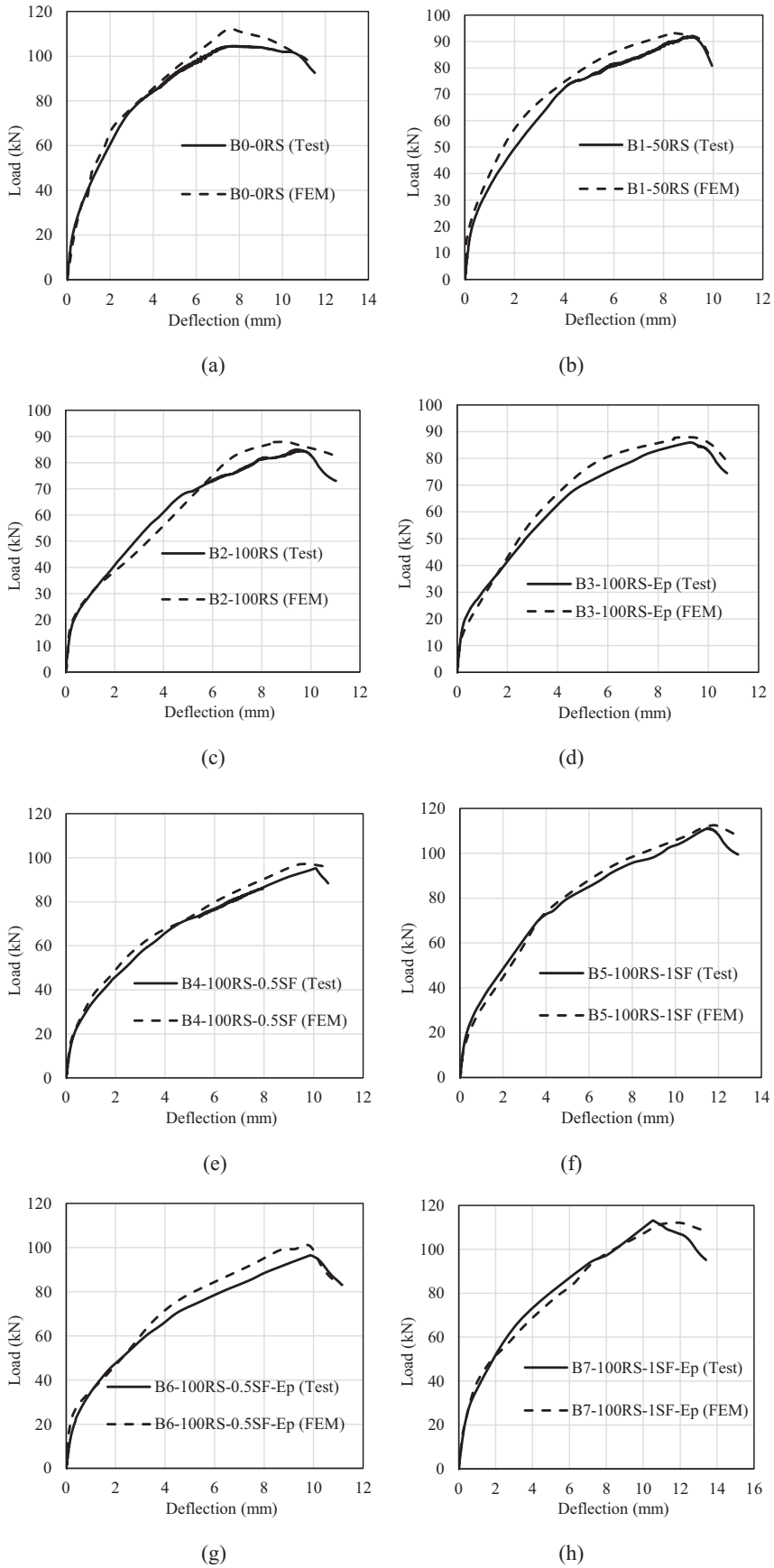

FIGURE 19 Load-deflection curves for all tested beams (experimental and finite element results). FEM, finite element models.

17517648, 0, Downloaded from https://onlinelibrary.wiley.com/doi/10.1002/suco.202300316 by Victoria Universiteit, Wiley Online Library on [22/11/2023]. See the Terms and Conditions (https://onlinelibrary.wiley.com/terms-and-conditions) on Wiley Online Library for rules of use; OA articles are governed by the applicable Creative Commons License

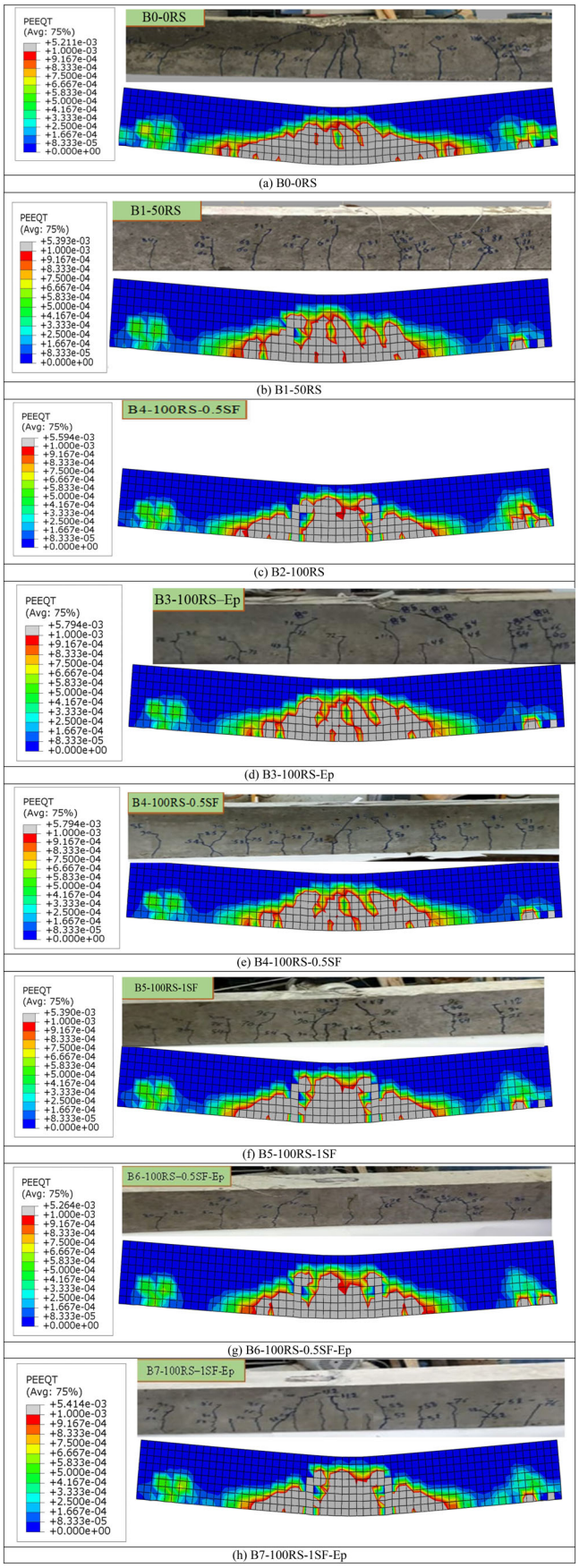

FIGURE 20 Comparison of predicted failure models with test observations.

the tested beams. The accuracy of the FE results is further validated by comparing the load–deflection curves of the tested beams in Figure 19. It is seen that there is a good agreement between the test and FE results. The failure modes of the tested beams are also compared with the FEM in Figure 20. A good match between the FEM and the test results can be observed.

6 | CONCLUSIONS

The flexural behavior of steel-fiber reinforced concrete beams incorporating reused longitudinal steel bars has been investigated experimentally and numerically. The test parameters were the replacement percentage of brand-new steel bars with reused ones, the coating of steel bars, and the volume fraction of SFs. The following conclusions can be drawn from this study:

a. Increasing the amount of reused steel bars in RC beams considerably decreases the load-carrying capacities of the beams but increases their corresponding deflections.
b. The more SFs added to the concrete, the higher the flexural strength and the larger the deflection at the ultimate load of the RC beam.
c. The zinc-rich epoxy used to coat the reused steel bars has no effects on the structural behavior of RC beams with and without SFs.
d. The ductility index of RC beams with and without reused steel bars increases with an increase in the amount of SFs in the concrete.
e. The use of reused steel bars and SFs increases the toughness of RC beams.
f. The FE model developed in this study can accurately predict the experimentally measured flexural behavior of RC beams with and without reused steel bars.

ACKNOWLEDGMENTS

The authors wish to thank the assistance of final-year students in carrying out some of the experimental work. Open access publishing facilitated by Victoria University, as part of the Wiley - Victoria University agreement via the Council of Australian University Librarians.

DATA AVAILABILITY STATEMENT

The data that support the findings of this study are available from the corresponding author upon reasonable request.

ORCID

Mohammed M. Attia https://orcid.org/0000-0001-8705-2513

17517648, 0, Downloaded from https://onlinelibrary.wiley.com/doi/10.1002/suco.202300316 by Victoria Universitaet, Wiley Online Library on [22/11/2023]. See the Terms and Conditions (https://onlinelibrary.wiley.com/terms-and-conditions) on Wiley Online Library for rules of use; OA articles are governed by the applicable Creative Commons License

Qing Quan Liang https://orcid.org/0000-0003-0333-2265
Basem O. Rageh https://orcid.org/0000-0002-1158-0739

REFERENCES

1. Elbehiry A, Elnawawy O, Kassem M, Zaher A, Mostafa M. FEM evaluation of reinforced concrete beams by hybrid and banana fiber bars (BFB). Case Stud Construct Mater. 2021;14:e00479.
2. Khalil A, Heniegal A, Attia MM. Nonlinear finite element analysis of steel fibers reinforced post-tensioned lightweight concrete beams. N Y Sci J. 2018;11:80–92.
3. Habert G, Miller SA, John VM, Provis JL, Favier A, Horvath A, et al. Environmental impacts and decarbonization strategies in the cement and concrete industries. Nat Rev Earth Environ. 2020;1(11):559–73.
4. Yazdani M, Kabirifar K, Frimpong BE, Shariati M, Mirmozaffari M, Boskabadi A. Improving construction and demolition waste collection service in an urban area using a simheuristic approach: a case study in Sydney, Australia. J Clean Prod. 2021;280:124138.
5. Tayeh BA, Hasaniyah M, Anza M, Abed M. Applying reused steel bars to new constructions (a case study in Gaza strip). J Eng Res Technol. 2018;5(1).
6. Ahmed HU, Faraj RH, Hilal N, Mohammed AA, Sherwani AFH. Use of recycled fibers in concrete composites: a systematic comprehensive review. Compos Part B Eng. 2021;215:108769.
7. Behbahani HP, Nematollahi B, Sam ARM, Lai F. Flexural behavior of steel-fiber-added-RC (SFARC) beams with C30 and C50 classes of concrete. Int J Sustain Construct Eng Technol. 2012;3(1):54–64.
8. Prakash R, Divyah N, Srividhya S, Avudaiappan S, Amran M, Naidu Raman S, et al. Effect of steel fiber on the strength and flexural characteristics of coconut shell concrete partially blended with fly ash. Materials. 2022;15(12):4272.
9. Mertol HC, Baran E, Bello HJ. Flexural behavior of lightly and heavily reinforced steel fiber concrete beams. Construct Build Mater. 2015;98:185–93.
10. Henager CH, Doherty TJ. Analysis of reinforced fibrous concrete beams. J Struct Div. 1976;102(1):177–88.
11. Fanaradelli TD, Rousakis TC. 3D finite element pseudodynamic analysis of deficient RC rectangular columns confined with fiber reinforced polymers under axial compression. Polymers. 2020;12(11):2546.
12. Rageh BO, El-Mandouh MA, Elmasry AH, Attia MM. Flexural behavior of rc beams strengthened with gfrp laminate and retrofitting with novelty of adhesive material. Buildings. 2022;12(9):1444.
13. Attia MM, El-Shaer MA, Shawky SM, Samaan MF. Replacement efficiency of steel reinforcement with FRB bars in RC beams under flexure load: experimental and FE study. Innov Infrastruct Solut. 2022;7(5):281.
14. Hamoda A, Emara M, Abdelazeem F, Ahmed M. Experimental and numerical analysis of RC beams strengthened with ECC and stainless steel strips. Mag Concr Res. 2022;75(5):251–70.
15. Hamoda A, Ahmed M, Sennah K. Experimental and numerical investigations of the effectiveness of engineered cementitious composites and stainless steel plates in shear strengthening of reinforced concrete beams. Struct Concr. 2022;24:2778–99.
16. El-Mandouh MA, Elsamak G, Rageh BO, Hamoda A, Abdelazeem F. Experimental and numerical investigation of one-way reinforced concrete slabs using various strengthening systems. Case Stud Construct Mater. 2023;18:e01691.
17. Hamoda A, Elsamak G, Emara M, Ahmed M, Liang QQ. Experimental and numerical studies of reinforced concrete beam-to-steel column composite joints subjected to torsional moment. Eng Struct. 2023;275:115219.
18. A370-19 standard test methods and definitions for mechanical testing of steel products. West Conshohocken, PA: ASTM International; 2019.
19. BS 5080-1:1993 Structural fixings in concrete and masonry. Method of test for tensile loadings. London, UK: British Standards Institute; 1993.
20. ACI Committee 544. ACI 544.4R-88: design considerations for steel fiber reinforced concrete. Farmington Hills, MI: American ConcreteInstitute; 1999.
21. Park R, Paulay T. Reinforced concrete structures. New York: John Wiley & Sons; 1991.
22. Ahmad SH, Barker R. Flexural behavior of reinforced high-strength lightweight concrete beams. Struct J. 1991;88(1):69–77.
23. Baran E, Akis T, Yesilmen S. Pull-out behavior of prestressing strands in steel fiber reinforced concrete. Construct Build Mater. 2012;28(1):362–71.
24. Altun F, Haktanir T, Ari K. Effects of steel fiber addition on mechanical properties of concrete and RC beams. Construct Build Mater. 2007;21(3):654–61.
25. Obaidat YT, Heyden S, Dahlblom O. The effect of CFRP and CFRP/concrete interface models when modelling retrofitted RC beams with FEM. Compos Struct. 2010;92(6):1391–8.
26. Teng J, Lam L, Chan W, Wang J. Retrofitting of deficient RC cantilever slabs using GFRP strips. J Compos Construct. 2000;4(2):75–84.
27. Wang J-J, Tao M-X, Nie X. Fracture energy-based model for average crack spacing of reinforced concrete considering size effect and concrete strength variation. Construct Build Mater. 2017;148:398–410.
28. Hibbitt K, Sorensen I. ABAQUS theory manual, user manual and example manual, version 6.7. Providence, RI: *Simulia*; 2000.
29. Gómez J, Torres L, Barris C. Characterization and simulation of the bond response of NSM FRP reinforcement in concrete. Materials. 2020;13(7):1770.
30. Mercan B, Schultz AE, Stolarski HK. Finite element modeling of prestressed concrete spandrel beams. Eng Struct. 2010;32(9):2804–13.

AUTHOR BIOGRAPHIES

Mohammed M. Attia, Civil and Architecture Constructions Department, Faculty of Technology and Education, Suez University, Egypt. Email: mohammed.mahmoudattia@suezuni.edu.eg.

17517648, 0, Downloaded from https://onlinelibrary.wiley.com/doi/10.1002/suco.202300316 by Victoria Universitaet, Wiley Online Library on [22/11/2023]. See the Terms and Conditions (https://onlinelibrary.wiley.com/terms-and-conditions) on Wiley Online Library for rules of use; OA articles are governed by the applicable Creative Commons License

Bassam Abdelsalam Abdelsalam, Civil and Architecture Constructions Department, Faculty of Technology and Education, Suez University, Egypt. Email: bassam.abdelsalam@suezuniv.edu.eg.

M. A Eita, The High Technological Institute, 10th of Ramadan City, Egypt. Email: mostafa.anter@hti.edu.eg.

Mizan Ahmed, Centre for Infrastructure Monitoring and Protection, School of Civil and Mechanical Engineering, Curtin University, Kent Street, Bentley, WA 6102, Australia. Email: mizan.ahmed@curtin.edu.au.

Qing Quan Liang, College of Sport, Health, and Engineering, Victoria University, PO Box 14,428, Melbourne, VIC 8001, Australia, qing.liang@vu.edu.au.

Basem O. Rageh, Civil Engineering Department, Delta Higher Institute for Engineering and Technology, Mansoura, Egypt. Email: bassem@dhiet.edu.eg.

How to cite this article: Attia MM, Abdelsalam BA, Eita MA, Ahmed M, Liang QQ, Rageh BO. Tests and finite element modeling of concrete beams reinforced with reused steel bars. Structural Concrete. 2023. https://doi.org/10.1002/suco.202300316

17517648, 0, Downloaded from https://onlinelibrary.wiley.com/doi/10.1002/suco.202300316 by Victoria Universitaet, Wiley Online Library on [22/11/2023]. See the Terms and Conditions (https://onlinelibrary.wiley.com/terms-and-conditions) on Wiley Online Library for rules of use; OA articles are governed by the applicable Creative Commons License